Materials Research Proceedings **16** (2020) 27-37 https://doi.org/10.21741/9781644900710-4

Nonlinear Optical Characterization of $CsPbBr_3$ Nanocrystals as a Novel Material for the Integration into Electro-Optic Modulators

Francesco Vitale [1,2 a *], Fabio De Matteis [1 b], Mauro Casalboni [1 c], Paolo Prosposito [1 d], Patrick Steglich[2,3 e], Viachaslau Ksianzou [2 f], Christian Breiler [2 g], Sigurd Schrader [2 h], Barbara Paci [4 i] and Amanda Generosi [4 j]

[1] Department of Industrial Engineering, University of Rome Tor Vergata, Via del Politecnico 1, Rome 00133, Italy

[2] Faculty of Engineering and Natural Sciences, Technical University of Applied Sciences Wildau, Wildau D-15745, Germany

[3] IHP-Leibniz Institute for Innovative Microelectronics, Frankfurt (Oder) D-15236, Germany

[4] ISM-CNR-Area di Ricerca di Tor Vergata, Via del Fosso del Cavaliere 100, Rome 00133, Italy

[a] francesco.vitale.mim@gmail.com, [b] fabio.dematteis@uniroma2.it, [c] casalboni@uniroma2.it, [d] paolo.prosposito@uniroma2.it, [e] steglich@ihp-microelectronics.com, [f] viachaslau.ksianzou@th-wildau.de, [g] christian.breiler@th-wildau.de, [h] schrader@th-wildau.de, [i] Barbara.Paci@ism.cnr.it, [j] amanda.generosi@ism.cnr.it

Keywords: $CsPbBr_3$ Nanocrystals, NLO Materials, Z-Scan, Kerr Effect, EOMs

Abstract. The present work is concerned with the investigation of the nonlinear optical response of green emissive $CsPbBr_3$ nanocrystals, in the form of colloidal dispersions in toluene, synthesized via a room-temperature ligand-assisted supersaturation recrystallization (LASR) method. After carrying out a preliminary characterization via X-Ray Diffraction (XRD) and Absorption and Photoluminescence (PL) Spectroscopies, the optical nonlinearity of the as-obtained colloids is probed by means of a single-beam Z-scan setup. Results show that the material in question, within the sensitivity of the experimental apparatus, exhibits a nonlinear refractive index n_2 that is the order of 10^{-15} cm^2/W. Moreover, a three-photon absorption mechanism (3PA) is postulated, according to the fitting of the recorded Z-scan traces and the fundamental absorption threshold, which turns out to be off resonance with twice the energy of the laser radiation. A figure of merit is, then, calculated as an indicator of the quality of the $CsPbBr_3$ nanocrystals as a candidate material for photonic devices, for instance, Kerr-like electro-optic modulators (EOMs).

Introduction

The past decade has been characterized by the flourishing development of fiber-integrated circuits and photonic devices [1] based on silicon-organic-hybrid (SOH) slot waveguides [2], namely two silicon rails separated by a submicrometric-wide slot infiltrated by a nonlinear optical (NLO) medium. Polymers and polymer-dye host-guest systems have been largely employed as active materials suitable for exploiting both the linear and quadratic electro-optic (EO) effects [3] [4] [5]. However it is well-known, that organic systems are usually affected by a remarkable two-photon absorption (2PA) that can diminish the effectiveness of the third-order nonlinearity, similarly to the case of silicon [6]. Moreover, the chemical and thermo-mechanical stability of organic materials is often undermined by the conditions at which the device is required to operate, especially at high temperatures. Hence, the quest for novel and promising

nonlinear optical active media that can meet these requirements is ongoing and lead halide perovskite nanocrystals are part of this framework.

Lead halide perovskites have emerged recently as promising materials for many applications in photovoltaics [7] [8] and optoelectronics [9] [10]. As concerns the field of photonics, latest works have shown some novel opportunities for the integration into nonlinear optical devices [11] [12], thanks to the low-cost fabrication and agile processability of these materials. Moreover, they exhibit remarkable electronic and optical properties such as relatively high values of the refractive index, broadband bandgap tunability, large optical gain and strong nonlinear response, which are enhanced at the nanoscale [13].

Experimental Section

Materials. Chemicals are employed as received, according to their original technical grade: CsBr (99.999%, Sigma-Aldrich), PbBr2 (99.999%, Sigma-Aldrich), DMF (≥ 99.5%, Carl Roth), DMSO (≥ 99.5%, Carl Roth), toluene (≥ 99.5%, Carl Roth), oleylamine (≥ 96%, Fisher Scientific) and oleic acid (90%, Fisher Scientific).

Synthesis of $CsPbBr_3$ nanocrystals. $CsPbBr_3$ nanocrystals are synthesized via room-temperature ligand-assisted supersaturation recrystallization (LASR) [14]. A mixed precursor solution is prepared by dissolving 0.04 mmol CsBr in 0.5 mL DMF and 0.04 mmol $PbBr_2$ in 0.5 mL DMSO. Alternatively, the dissolution of salts into the aprotic polar solvents is reversed, namely CsBr in DMSO and $PbBr_2$ in DMF (preparation B). Afterwards, the surface ligands, namely oleylamine (20 μL) and oleic acid (10 μL), are added to the as-obtained 1 mL precursor solution: they help to control the size of the nanocrystals and to disperse them into the anti-solvent. Stirring at 70-75°C for ca. 30 min is accomplished for promoting the complete dissolution of the salts. Hence, 0.25 mL of precursor solution are swiftly injected toluene which acts as the anti-solvent, i.e. a poor solvent for the ions from the precursor salts. The drop between the precursor solubility into the aprotic polar solvents and that into toluene, thus, promotes the formation of a supersaturated state in which the recrystallization of the perovskite phase takes place. Agitation is kept for approximately 1 min, that is the estimated time for the complete formation of nanocrystal [15]. If the vial is irradiated under UV light, a green bright emission is observed, as an indicator for the occurred recrystallization of the perovskite phase.

X-Ray Diffraction Measurements. XRD measurements are performed in reflection mode on a Panalytical Empyrean Diffractometer, using the K_α fluorescence line of a Cu-anode emitting tube. Bragg- Brentano configuration is used as the incident optical pathway (0.25°-0.5°) divergent slits and a solid state hybrid Pix'cel 3D detector, working in 1D linear mode, accomplishes the detection. Samples are studied in the range $10° < 2\theta < 50°$, in the form of thin films drop-cast on glass substrates, with an estimated thickness of few microns.

Spectral Measurements. Absorption spectra are recorded by means of a double beam spectrophotometer (Perkin Elmer Lambda-19), while photoluminescence (PL) measurements are performed via excitation of the 458 nm line of an Ar^+ laser and collected by a compact spectrophotometer (Flame, OceanOptics). Samples are probed in the form of the as-obtained colloids collected inside 1 mm wide glass cuvettes (Hellma® Analytics).

Z-Scan Measurements. The single-beam Z-scan setup is shown in Figure 1. The laser radiation employed for the analysis is the fundamental wavelength (λ = 1064 nm) of a Nd:YAG solid state laser, passively Q-switched via saturable absorber: the nominal pulse duration is $\tau_p \approx$ 30 ps at a repetition rate of $\nu \approx$ 10 Hz. The wavelength chosen for the analysis is assessed to be suitable on account of the fact that the fundamental harmonic of the Nd:YAG is rather adjacent to the telecom wavelengths λ = 1300 nm and λ = 1550 nm. It seems reasonable to expect that the variation of the NLO coefficients in this wavelength range be small, if compared to that for shorter wavelengths.

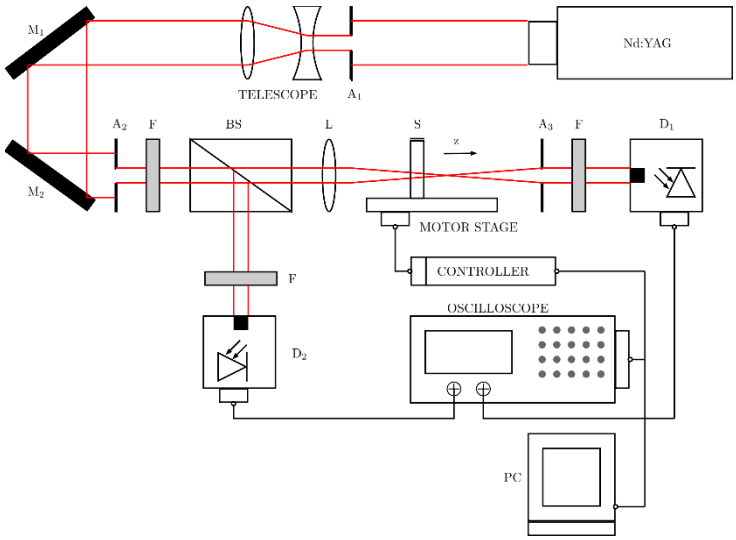

***Figure 1**: Schematic of the single-beam Z-scan apparatus. The acquisition is accomplished through an oscilloscope, whose readout is monitored via LabVIEW. A linear controller interfaced with the PC remotely controls the motor stage: this displaces the sample towards the detector D_1, namely along the positive z-direction.*

The output laser radiation passes through a telescope, which acts as a beam expander and is used for improving the beam quality. Consequently, two mirrors (M_1 and M_2) deflect the beam onto the Z-scan line, where the beam alignment is controlled by the apertures A_2 and A_3. The beam splitter (BS) splits the beam in two parts: ≈ 60% is sent to the probe detector D_1, while ≈ 40% to the reference detector D_2. A converging lens (L) is used for focusing the beam on the sample, while filters (F) are used for attenuating the laser energy and for preventing the saturation of photodetectors, namely, two Si PIN photodiodes with a rise time $t_R \approx$ 35 ns.

Results and Discussion

Spectral and XRD Characterization. A signature for the formation of green emissive $CsPbBr_3$ nanocrystals is represented by the emission peak appearing at 520 nm, as reported in Fig. 2. The fluorescence was excited at 458 nm (edge-filter at 480 nm). The absorption threshold occurring **around 500 nm is usually observed in nanocrystals smaller than 50 nm [15] [16] [17].**

Materials Research Forum LLC
https://doi.org/10.21741/9781644900710-4

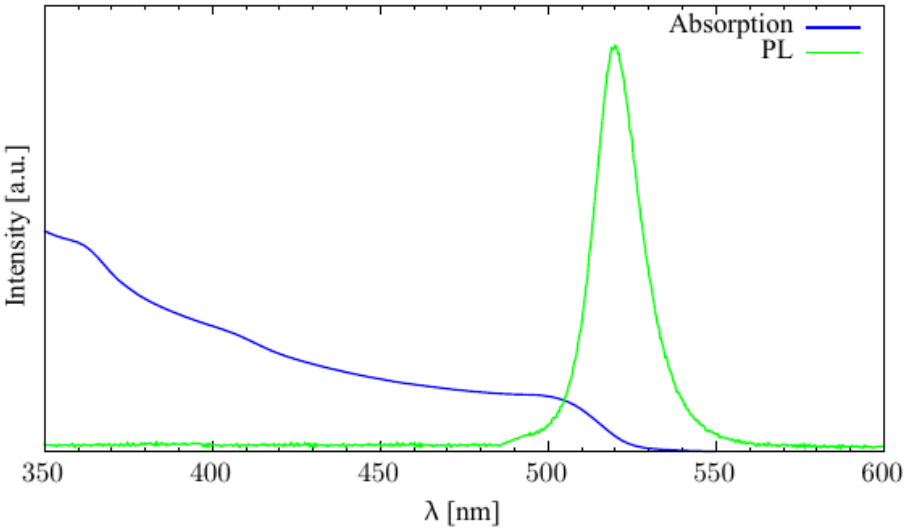

***Figure 2**: Typical absorption and PL spectra of green emissive CsPbBr3 NCs colloids prepared via LASR, showing the characteristic absorption threshold occurring at wavelengths around 500 nm, while a quite strong emission is seen to be peaked at 519 nm. Spectra are reported on the same intensity scale only for qualitative purposes.*

The XRD spectra of the perovskite thin films are shown in Fig. 3: both samples present the dominant $CsPbBr_3$ monoclinic phase (ICDD N0. 00- 018- 0364), characterized by lattice constants a = b = 5.82 Å and c = 5.87 Å, and angles $\alpha = \beta = 90°$ and $\gamma = 89.65°$. This phase is characterized by the signature peaks at $2\theta = 15.1°$ and $2\theta = 15.2°$, referred to the diffraction from crystallographic planes (001) and (100) respectively; $2\theta = 21.5°$ and $2\theta = 21.7°$ from planes (110) and (-110); $2\theta = 30.4°$ and $2\theta = 30.7°$, from planes (002) and (200).

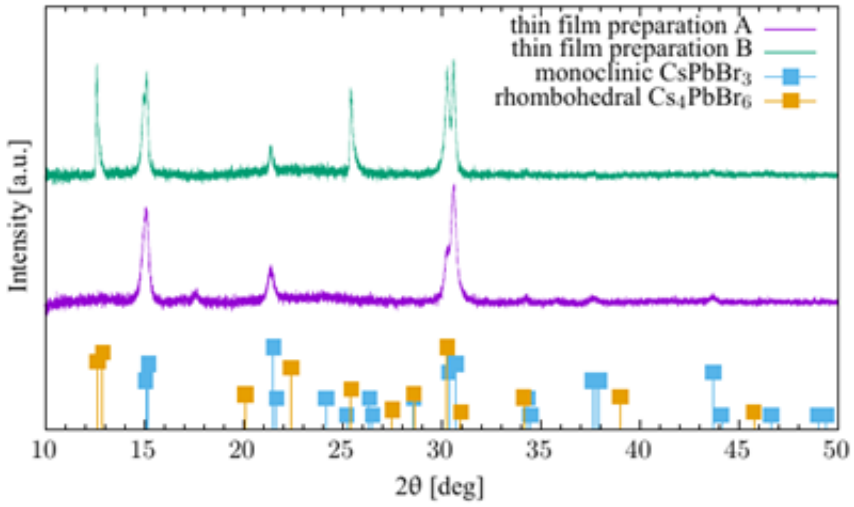

***Figure 3**: XRD spectra of thin films from preparations A and B, along with the labeling (colored squares) of XRD reflections from $CsPbBr_3$ monoclinic and rhombohedral Cs_4PbBr_6 phases*

Interestingly, the spectrum referring to preparation B exhibits also fingerprinting peaks of the rhombohedral Cs_4PbBr_6 phase (ICDD No. 01- 073- 2478) with lattice constants a = b = 13.73 Å and c = 17.32 Å, and angles $\alpha = \beta = 90°$ and $\gamma = 120°$, even if the monoclinic phase is still predominant. We attribute this to the higher reactive amount of Cs^+ in preparation B, which tends to react with $PbBr_2$ dissolved in DMF to form Cs_4PbBr_6, confirming the results of Yang et al. [16]. However, only the pure $CsPbBr_3$ NCs colloids obtained from preparation A are devoted to the Z-scan measurements, since, at this point of the analysis, understanding the contribution of the Cs_4PbBr_6 phase to the NLO activity of the nanocrystals is beyond the scope of this work. The average size of the ordered polycrystalline domains has been estimated by means of the Scherrer formula. Peak analysis yields a mean grain size of $D_A = 23 \pm 1$ nm and $D_B = 35 \pm 1$ nm for the $CsPbBr_3$ monoclinic phase resulting from the two preparations, comparable to those reported in [16] [17].

NLO Characterization via Z-Scan: Closed-Aperture Configuration**.** CS_2 has been used to calibrate the as-built single-beam Z-Scan setup – as originally developed by Sheik-Bahae et al. [18] - in closed-aperture configuration (CA). CS_2 is a standard material for this type of measurements whose nonlinear refractive index is well-known in the literature [19] [20]: $n_2 = (3.1 \pm 0.2) \cdot 10^{-14}$ cm^2/W. To the best of the beam quality optimization, laser energy fluctuations are estimated to be in between 10 - 15%: a cuvette filled with CS_2 is, thus, probed for calibrating the irradiance I_0. Data acquisition is performed by using a 10 cm focal length lens, a diaphragm with aperture radius $r_a \approx 0.5$ mm and linear transmittance $S \approx 0.4$ %, which is sufficiently small to consider the limiting case $S \to 0$ for the CA peak-valley transmittance ΔT_{CA}:

$$\Delta T_{CA} \cong 0.406|\Delta\Phi_0|. \tag{1}$$

$\Delta\Phi_0$ is the time-averaged nonlinear phase shift:

$$\Delta\Phi_0 = k\frac{n_2}{\sqrt{2}}I_0 L_{eff} \tag{2}$$

where k is the radiation wavenumber and L_{eff} the optical path inside the cuvette. A *z*-resolution of $\delta z = 0.5$ mm is found to be a good compromise in between the reproducibility of measurements and the irradiation time that samples are subject to, in order to prevent the potential build-up of thermal effects.

The experimental data are fitted with the theoretical curve for the closed-aperture configuration transmittance [16]:

$$T_{CA}(z,\Delta T) = a + 4\left(\frac{z+b}{z_R}\right)\frac{\Delta T}{0.406}\frac{1}{\left[\left(\frac{z+b}{z_R}\right)^2+9\right]\left[\left(\frac{z+b}{z_R}\right)^2+1\right]} \tag{3}$$

where $\Delta\Phi_0$is expressed by Eq. (2), z_R is the beam Rayleigh length while *a* and *b* are scaling factors: the former accounts for the normalized transmittance offset and the latter for the focus position. Average pulse energy and beam diameter are monitored by using a beam profiler (WinCamD): the beam waist is estimated to be $w_0 = 24\pm 1$ μm at an irradiance of $I_0 = 14 \pm 2$ GW/cm^2.

Z-scan measurements on solutions and colloids are affected by the solvent effect: thus, it is necessary to accomplish a scan on the solvent as well, in order to subtract any nonlinear contribution from that of the entire solution. CA scans of the solvent (toluene) and the $CsPbBr_3$

NCs colloidal dispersions at three different concentrations (namely 1.5, 2.5 and 4 mM) are shown in Fig. 4.

It must be noticed that when increasing the concentration, scattering processes become predominant: this is apparent from the "humps" emerging in the linear region and, especially, in the asymmetry - with respect to the focus position - affecting the whole Z-scan trace. Fitted ΔT and calculated n_2 values for the perovskite NCs are reported in Tab. 1.

The magnitude and the sign of the NLO coefficients usually depend on several factors:

- Radiation-related: peak power and repetition rate, when too high, usually lead to negative nonlinearities and saturation that can be ascribed to the build-up of thermo-optic effects. Another contribution arises, obviously, from the operating wavelength due to the dispersion of the NLO coefficients.
- Medium-related: degree of crystallinity, morphology and size.

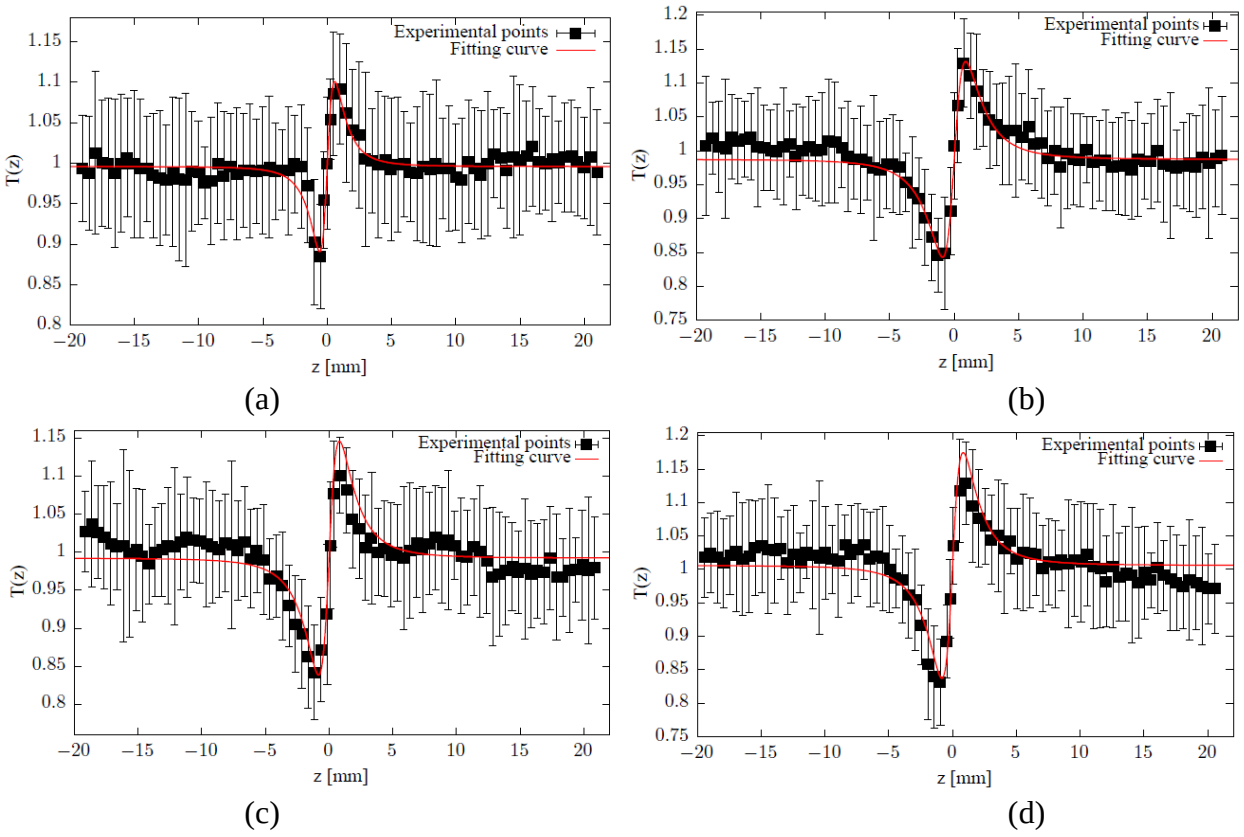

***Figure 4**: CA Z-scan traces of $CsPbBr_3$ NCs colloidal dispersions in toluene at a) 0 mM, b) 1.5 mM, c) 2.5 mM, d) 4 mM.*

As a matter of fact, it is usually difficult to compare NLO coefficients obtained from a Z-scan when not taking into account all of the above-mentioned parameters. To the best of our knowledge, although the literature concerning Z-scan measurements of colloidal $CsPbBr_3$ NCs is still relatively scarce, the n_2 values reported in this work are in good agreement with the results of Liu et al. [21], who found a nonlinear refractive index $n_2 \approx 0.7 \cdot 10\text{-}14$ cm^2/W for green emissive $CsPbBr_3$ nanocrystals (D = 21.4 nm) at 787 nm.

Materials Research Forum LLC
https://doi.org/10.21741/9781644900710-4

NLO Characterization via Z-Scan: Open-Aperture Configuration In order to investigate NLA, the aperture A_3 placed in front of the detector D_1 is fully opened (S = 100%). Fig. 5 shows the OA Z-scan traces for the perovskite colloidal dispersions at the same three different concentrations as for CA and for toluene.

***Table 1**: ΔT and calculated n_2 values for the perovskite NCs.*

Conc. [mM]	ΔT	$n_{2,P}$[·10^{-14} cm^2/W]
1.5	0.29 ± 0.01	0.4 ± 0.1
2.5	0.31 ± 0.02	0.5 ± 0.1
4	0.34 ± 0.02	0.6 ± 0.1

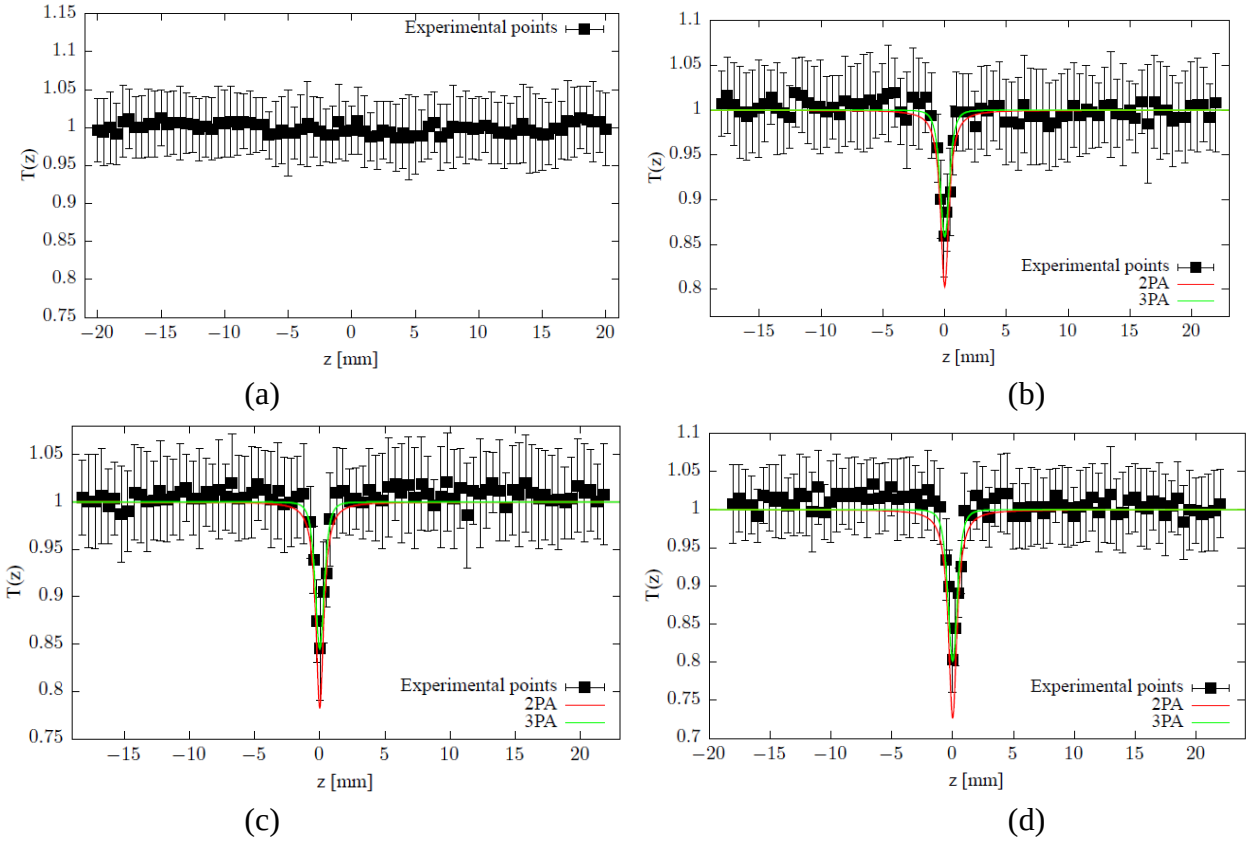

***Figure 5**: OA Z-scan traces of CsPbBr3 NCs colloidal dispersions in toluene at a) 0 mM, b) 1.5 mM, c) 2.5 mM, d) 4 mM.*

Since the solvent exhibits a negligible nonlinear absorption within the sensitivity of the as-built setup, the NLA coefficients returned by the fit, are specifically referred to the perovskite NCs. Experimental data are fitted with the theoretical curves referred to two- and three-photon absorption transmittance [22]:

$$T_{OA}(z,\beta_2) = \sum_{m=0}^{\infty} \frac{(-1)^m}{(m+1)^{\frac{3}{2}}} \left[\frac{\beta_2 I_0 L_{eff}}{1+z^2/z_R^2}\right]^m \quad ; \tag{4.a}$$

$$T_{OA}(z,\beta_3) = \sum_{m=1}^{\infty} \frac{(-1)^{m-1}}{(2m-1)!(2m-1)^{\frac{1}{2}}} \left[\frac{\sqrt{2\beta_3 I_0^2 L_{eff}^{(2)}}}{1+\frac{(z+b)^2}{z_R}} \right]^{2(m-1)} \quad (4.b)$$

where the effective lengths can be both approximated with the cuvette width at λ = 1064 nm, and $\beta_2$and β_3 represent the 2PA and 3PA coefficients respectively. A three-photon absorption mechanism occurring in perovskite NCs is, thus, postulated, as evidenced from the fact that, within the accuracy guaranteed by the *z* resolution, the 3PA theoretical curve fits the experimental points better than the 2PA curve. This is reasonable when also considering that the wavelength corresponding to twice the laser energy $\lambda_{2\omega}$ = 532 nm falls outside of the absorption band, while the wavelength corresponding to thrice the laser energy $\lambda_{3\omega} \approx$ 355 nm is clearly inside the resonance region.

However, it must be clarified that in order to corroborate this hypothesis, further investigation is required. For instance, a useful tool is represented by a wavelength-dependent Z-scan analysis, in order to probe the dispersion of the multiphoton absorption coefficients, which follow specific scaling rules as a function of the radiation energy [23] [24]. The β_3 values returned by the fit are shown in Table 2.

***Table 1**: β_3 values for perovskite colloidal dispersions at different concentrations.*

Conc. [mM]	$\beta_{3,P}$[·10^{-2} cm^3/GW^2]
1.5	1.2 ± 0.2
2.5	1.4 ± 0.2
4	1.8 ± 0.2

A further proof of an apparent 3PA process is given by the work of Manzi et al. [25], who found a 2PA-to-3PA transition at about 1030 nm by studying the nonlinear absorption-induced PL in green emissive $CsPbBr_3$ nanocrystals (*D* = 10 – 15 nm) by means of a 15ps-pulsed excitation ensured by a tunable laser working in the range 680 – 1080 nm.

Conclusions

We have presented an assessment of the quality of green emissive $CsPbBr_3$ nanocrystals as a potential active medium for electro-optic modulators and other photonic devices exploiting the Kerr effect, on the basis of the NLO coefficients yielded by the Z-scan analysis. Besides the remarkable magnitude of the nonlinear refraction, the postulated 3PA mechanism in the mid-IR range is, indeed, preferable – from a probabilistic point of view - to a 2PA process, which is usually observed in organic materials, within the computation of the optical losses inside a waveguide. Furthermore, the dispersion into an optically-inactive polymer matrix can be also considered as a good strategy for both preventing aggregation mechanism among the perovskite nanocrystals and at the same time improving their stability once deposited into the waveguide.

Acknowledgments

Research supported by Regione Lazio through Progetto di ricerca 85-2017-15125, funded according to L.R.13/08.

References

[1] G. Alimonti, G. Ammendola, A. Andreazza, D. Badoni, V. Bonaiuto, M. Casalboni, F. De Matteis, A. Mai, G. Paoluzzi, P. Prosposito, A. Salamon, G. Salina, E. Santovetti, F. Sargeni, F. Satta, S. Schrader and P. Steglich, "Use of Silicon Photonics Wavelength Multiplexing Techniques for Fast Parallel Readout in High Energy Physics," *Nuclear Instruments and Methods in Physics Research Section A: Accelerators, Spectrometers, Detectors and Associated Equipment,* vol. 936, no. 21, pp. 601-603, 2019. https://doi.org/10.1016/j.nima.2018.09.088

[2] V. Almeida, Q. Xu, C. Barrios and M. Lipson, "Guiding and Confining Light in Void Nanostructure," *Optics Letters,* vol. 29, no. 11, pp. 1209-1211, 2004. https://doi.org/10.1364/OL.29.001209

[3] P. Steglich, C. Mai, D. Stolarek, S. Lischke, S. Kupijai, C. Villringer, S. Pulwer, F. Heinrich, J. Bauer, S. Meister, D. Knoll and M. Casalboni, "Novel Ring Resonator Combining Strong Field Confinement With High Optical Quality Factor," *IEEE Photonics technology Letters,* vol. 27, no. 20, pp. 2197-2200, 2015. https://doi.org/10.1109/LPT.2015.2456133

[4] P. Steglich, "Silicon-On-Insulator Slot Waveguides: Theory and Applications in Electro-Optics and Optical Sensing," in *Emerging Waveguide Technology,* IntechOpen, 2018, pp. 187-210. https://doi.org/10.5772/intechopen.75539

[5] P. Steglich, C. Mai, C. Villringer, S. Pulwer, M. Casalboni, S. Schrader and A. Mai, "Quadratic Electro-Optic Effect in Silicon-Organic Hybrid Slot-Waveguides," *Optics Letters,* vol. 43, no. 15, pp. 3598-3601, 2018. https://doi.org/10.1364/OL.43.003598

[6] J. Leuthold, C. Koos, W. Freude, L. Alloatti, R. Palmer, D. Korn, M. Jazbinsek, J. Pfeifle, M. Lauermann, R. Dinu, M. Waldow, T. Wahlbrink, J. Bolten, M. Fournier, H. Yu, S. Wehrli, J. Fedeli, P. Gunter and W. Bogaerts, "Silicon-Organic Hybrid Electro-Optical Devices," *IEEE Journal of Selected Topics in Quantum Electronics,* vol. 19, no. 6, pp. 114-120, 2013. https://doi.org/10.1109/JSTQE.2013.2271846

[7] H. Snaith, "Perovskites: the Emergence of a New Era for Low-Cost, High-Efficiency Solar Cells," *Journal of Physical Chemistry Letters,* vol. 4, no. 21, pp. 3623-3630, 2013. https://doi.org/10.1021/jz4020162

[8] M. Green, A. Ho-Baillie and H. Snaith, "The Emergence of Perovskite Solar Cells," *Nature Photonics,* vol. 8, no. 7, p. 506, 2014. https://doi.org/10.1038/nphoton.2014.134

[9] F. Deschler , M. Price, S. Pathak, L. Klintberg, D. Jarausch, R. Higler, S. Hüttner, T. Leijtens, S. Stranks, H. Snaith and M. Atatüre, "High Photoluminescence Efficiency and Optically Pumped Lasing in Solution-Processed Mixed Halide," *Journal of Physical Chemistry Letters,* pp. 1421-1426, 2014. https://doi.org/10.1021/jz5005285

[10] S. Stranks and H. Snaith, "Metal-Halide Perovskites for Photovoltaic and Light-Emitting Devices," *Nature Nanotechnology,* vol. 10, no. 5, p. 391, 2015. https://doi.org/10.1038/nnano.2015.90

[11] W. Mao, J. Zheng, C. Zhang, A. Chesman, Q. Ou, J. Hicks, F. Li, Z. Wang, B. Graystone, T. Bell and M. Rothmann, "Controlled Growth of Monocrystalline Organo-Lead Halide

Perovskite and its Application in Photonic Devices," *Angewandte Chemie,* vol. 56, no. 41, pp. 12486-12491, 2017. https://doi.org/10.1002/anie.201703786

[12] A. Chanana, X. Liu, C. Zhang, Z. Vardeny and A. Nahata, "Ultrafast Frequency-Agile Terahertz Devices using Methylammonium Lead Halide Perovskites," Sci. Adv. 4(5), 7353 (2018).," *Science Advances,* vol. 4, no. 5, p. 7353, 2018. https://doi.org/10.1126/sciadv.aar7353

[13] Q. Akkerman, G. Rainò, M. Kovalenko and L. Manna, "Genesis, Challenges and Opportunities for Colloidal Lead Halide Perovskite Nanocrystals," *Nature Materials,* vol. 17, no. 5, p. 394, 2018. https://doi.org/10.1038/s41563-018-0018-4

[14] X. Li, Y. Wu, S. Zhang, B. Cai, Y. Gu, J. Song and H. Zeng, "CsPbX3 Quantum Dots for Lighting and Displays: Room-Temperature Synthesis, Photoluminescence Superiorities, Underlying Origins and White Light-Emitting Diodes," *Advanced Functional Materials,* vol. 26, no. 15, pp. 2435-2445, 2016. https://doi.org/10.1002/adfm.201600109

[15] S. Seth and A. Samanta, "A Facile Methodology for Engineering the Morphology of CsPbX3 Perovskite Nanocrystals under Ambient Condition," *Scientific Reports,* vol. 6, p. 37693, 2016. https://doi.org/10.1038/srep37693

[16] L. Yang, D. Li, C. Wang, W. Yao, H. Wang and K. Huang, "Room-Temperature Synthesis of Pure Perovskite-Related Cs4PbBr6 Nanocrystals and their Ligand-Mediated Evolution into Highly Luminescent CsPbBr3 Nanosheets," *Journal of Nanoparticle Research,* vol. 19, no. 7, p. 258, 2017. https://doi.org/10.1007/s11051-017-3959-7

[17] F. De Matteis, F. Vitale, S. Privitera, E. Ciotta, R. Pizzoferrato, A. Generosi, B. Paci, L. Di Mario, J. Pelli Cresi, F. Martelli and P. Prosposito, "Optical Characterization of Cesium Lead Bromide Perovskites," *Crystals,* vol. 9, p. 280, 2019. https://doi.org/10.3390/cryst9060280

[18] M. Sheik-Bahae, A. Said and E. Van Stryland, "High-Sensitivity, Single-Beam n2 Measurements," *Optics Letters,* vol. 14, no. 17, pp. 955-957, 1989. https://doi.org/10.1364/OL.14.000955

[19] M. Sheik-Bahae, A. Said, H. Wei, D. Hagan and E. Van Stryland, "Sensitive Measurement of Optical Nonlinearities using a Single Beam," *IEEE Journal of Quantum Electronics,* vol. 26, no. 4, pp. 760-769, 1990. https://doi.org/10.1109/3.53394

[20] E. Van Stryland and M. Sheik-Bahae, " Z-Scan Measurements of Optical Nonlinearities," in *Characterization Techniques and Tabulations for Organic Nonlinear Materials*, Marcel Dekker Inc., 1998, pp. 671-708.

[21] S. Liu, C. Guixiang, H. Yunyu, S. Lin, Y. Zhang, M. He, W. Xiang and X. Liang, "Tunable Fluorescence and Optical Nonlinearities of All Inorganic Colloidal Cesium Lead Halide Perovskite Nanocrystals," *Journal of Alloys and Compounds,* vol. 724, pp. 889-896, 2017. https://doi.org/10.1016/j.jallcom.2017.06.034

[22] J. He, Y. Qu, H. Li, J. Mi and W. Ji, "Three-Photon Absorption in ZnO and ZnS Crystals," *Optics Express,* vol. 13, no. 23, pp. 9235-9247, 2005. https://doi.org/10.1364/OPEX.13.009235

[23] B. Wherrett, "Scaling Rules for Multiphoton Interband Absorption in Semiconductors," *Journal of the Optical Society of America B,* vol. 1, no. 1, pp. 67-72, 1984. https://doi.org/10.1364/JOSAB.1.000067

[24] H. Brandi and C. De Araujos, "Multiphoton Absorption Coefficients in Solids: a Universal Curve," *Journal of Physics C: Solid State Physics,* vol. 16, no. 30, p. 5929, 1983. https://doi.org/10.1088/0022-3719/16/30/022

[25] A. Manzi, Y. Tong, J. Feucht, E. Yao, L. Polavarapu, A. Urban and J. Feldmann, "Resonantly Enhanced Multiple Exciton Generation through Below-Band-Gap Multi-Photon Absorption in Perovskite Nanocrystals," *Nature Communications,* vol. 9, no. 1, p. 1518, 2018. https://doi.org/10.1038/s41467-018-03965-8